ARTICLE NO. 79-1169R

Engine/Aircraft Afterbody Interactions: Recommended Testing Techniques Based on YF-17 Experience

A. E. Fanning*
Air Force Aero Propulsion Laboratory, Wright-Patterson AFB, Ohio
and
E. J. Lucas†
ARO, Inc., Arnold Air Force Station, Tenn.

Installation losses are deviations from the ideal of interactions between propulsion system flows and external aerodynamics. A summary of initial results of an extensive experimental effort to identify and reduce the uncertainties introduced by the methods used to predict these losses is presented. The test techniques used during this effort are presented with data to substantiate their validity. The results of testing two different scale, wind-tunnel models are used to define the effects of characteristic Reynolds number and model scale. The techniques used to correct wind-tunnel data to free-flight conditions are presented and the results compared to flight test data. Comparisons of surface static pressure distributions and integrated axial pressure forces are included. Based upon these comparisons, it was concluded that accurate predictions of subsonic full-scale, flight vehicle nozzle/afterbody installation losses are within the state-of-the-art using wind-tunnel testing of subscale models. This accuracy can be achieved using currently available facilities, test techniques, and analysis methods, if more care than has been routinely applied is exercised. Particular emphasis should be placed on determining the effects of tunnel calibration errors, support system interference, Reynolds number, and model scale.

Nomenclature

A_x = area, projected on a plane normal to body longitudinal axis
$CAPP$ = coefficient of axial force resulting from pressure distribution, referenced to maximum cross-sectional area A_{10}
$CAPW$ = coefficient of axial force resulting from pressure distribution, referenced to wing reference area S_w
$CDPA$ = coefficient of drag force resulting from pressure distribution, referenced to nacelle cross-sectional area at nozzle connect plane A_{11}
DCP = difference in static pressure coefficient
F_x = force, applied parallel to body longitudinal axis
L = length of body along longitudinal axis
M = Mach number of flow, relative to body
$\dot{m}$ = rate of mass flow
NPR = nozzle pressure ratio, P_9/P_{so}
P = pressure, total, relative to body
P_s = pressure, static
PN/PT = data point reference number, (part number/point number)
Re_L,REL = characteristic Reynolds number, based upon body length L
S_w = area, wing reference
u = velocity, relative to body, parallel to longitudinal axis
X = distance along body longitudinal axis
α = angle of attack
δ_h = horizontal stabilator deflection

Station Designation Subscripts

o = freestream
c = inlet capture plane
9 = nozzle exit plane
9_i = plume ideal expansion plane
10 = plane of body maximum cross-sectional area
11 = nozzle connect plane

Subscripts Applied to CAPP, CAPW, and CDPA

none = afterbody and nozzle only
FB = forebody only
T = total; forebody, afterbody, and nozzle

Introduction

INSTALLATION effects are the result of losses associated with the interactions between the inlet streamtube and the aircraft forebody flowfield or between the exhaust plume and the aircraft afterbody and nozzle flowfield. An understanding of the fundamental aspects governing these interactions may be obtained by considering the simplified engine and nacelle combination shown in Fig. 1. In this example, the force applied to the nacelle and engine combination can be shown to be numerically equal to the change in momentum between a location in the inlet streamtube where the flow is at ambient conditions and a location in the exhaust plume where the

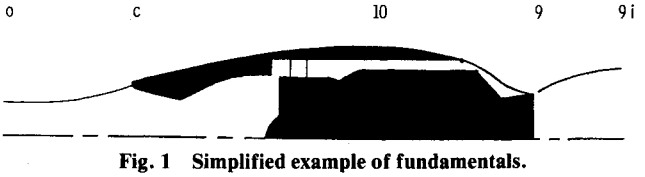

Fig. 1 Simplified example of fundamentals.

Presented as Paper 79-1169 at the AIAA/SAE/ASME 15th Joint Propulsion Conference, Las Vegas, Nev., June 18-20, 1979; submitted Aug. 3, 1979; revision received Jan. 18, 1980. This paper is declared a work of the U.S. Government and therefore is in the public domain.

Index categories: Aerodynamics; Testing, Flight and Ground; Air-breathing Propulsion

*Technical Manager, Turbine Engine Performance Group, Turbine Engine Division (Presently Research Associate, Frank J. Seiler Laboratory, U.S. Air Force Academy, Colo.) Member AIAA.

†Project Engineer, Projects Branch, Propulsion Wind Tunnel.

plume has been expanded to ambient pressure, modified by the two terms within brackets:

$$\sum F_x = (\dot{m}u)_{9i} - (\dot{m}u)_o$$

$$- \left[\int_o^c (P_s - P_{so})\,dA_x + \int_c^{10} (P_s - P_{so})\,dA_x\right]$$

$$- \left[\int_{10}^{9} (P_s - P_{so})\,dA_x + \int_9^{9i} (P_s - P_{so})\,dA_x\right]$$

The first set of terms within brackets accounts for the forces applied along the boundary of the expanding inlet streamtube and the drag on the aircraft forebody. The terms within the second set of brackets represent the drag force applied to the aircraft afterbody and the external surfaces of the engine nozzle and the forces applied to the exhaust plume as it expands or contracts to adjust to ambient static pressure.

The recent experimental investigations of Spratley[1] have demonstrated that for bodies of fineness ratio and cross-sectional area distribution representative of current air superiority fighter aircraft, the forebody drag is very nearly independent of the afterbody configurations in the Mach number range of 0.60 to 1.40. The implication of this result is that for the purposes of defining the fundamental interactions between the forebody and the propulsion streamtube, little accuracy of representation is lost by considering the forebody to be uncoupled from the afterbody. Thus the inlet streamtube and the forebody may be represented by an infinite body with a change in cross-sectional area to coincide with the expansion or contraction of the inlet streamtube and the configuration of the forebody. Introducing the further assumptions of isentropic, incompressible, inviscid external flow, it can be shown that both the sum of the terms within the first set of brackets and the sum of the terms within both sets of brackets are identically equal to zero. The implicit conclusion, that the sum of the terms within the second set of brackets must remain identically equal to zero, provides a basis for identifying the results of the fundamental interaction between the exhaust plume and the external flowfield around the afterbody, external nozzle, and exhaust plume. For the sum of the terms within the second set of brackets to remain equal to zero, the nozzle and afterbody drag must vary as a function of the degree of expansion which must take place external to the engine nozzle. In addition, it can be seen that in the simplified example the drag applied to the aircraft afterbody and nozzle is independent of nozzle closure, if the exhaust at the nozzle is maintained at fully expanded conditions. These two phenomena form the fundamental interactions between the aircraft afterbody/engine nozzle and the exhaust plume. Real world effects cause the sum of the terms within this second set of brackets to be nonzero and the actual value of these terms characterize the installation losses associated with the interaction between engine exhaust plume and aircraft afterbody and nozzle flowfield.

The results of the simplified ideal example given here are useful as a benchmark against which performance can be measured, since the performance obtained in the isentropic case is not likely to be exceeded. In addition, the example is useful as a method of identifying the fundamental trends which will likely be altered by loss mechanisms, but not so much as to make them totally invalid. However, the example is of little value in making quantified predictions of the installation losses experienced by an aircraft in flight. In order to make quantified predictions, it is necessary to resort to more sophisticated analysis and ultimately to wind-tunnel testing of subscale models. The subject of this paper is the results of work done to define and improve the accuracy with which the nozzle and aircraft afterbody installation effects can be predicted based upon wind-tunnel testing of subscale models.

Quantitative predictions of aircraft afterbody and nozzle installation losses are usually based upon wind-tunnel testing of subscale models. Although other variables may be of significance, usually interest is centered on determining the effects of variations in nozzle closures and exhaust pressure ratio, NPR. In order to determine the effect of nozzle pressure ratio, high-pressure air is supplied to the model through the support system and then exhausted through the nozzles to simulate the exhaust plume. The effects of variation in nozzle closure and internal area ratio are determined by simulating the closure, internal area ratio, and external contour of the variable, convergent-divergent nozzle normally found on fighter aircraft through the use of interchangeable nozzle hardware of various fixed closures.

Since wind-tunnel testing of subscale models provides only a simulation of full-scale performance, some uncertainty regarding the accuracy of predictions of flight performance based upon such data is always present. One cause of such uncertainty is the failure to simulate flight Reynolds numbers during wind-tunnel testing. Data obtained during a series of carefully conducted wind-tunnel and flight experiments indicated that nozzle and afterbody pressure drag was a strong function of characteristic Reynolds number.[2] Data from these tests, shown in Fig. 2, indicate predictions of full-scale, flight performance based upon wind-tunnel testing of subscale models can be significantly in error, if the effects of variations in characteristic Reynolds number are not determined. Because of the significant potential error which might be introduced by not determining the effects of Reynolds number, efforts to identify this effect were included in an existing program.

Technical Approach

The results reported in this paper were extracted from the results of a program with the following objective: Provide adequate capability to accurately predict full-scale, flight vehicle, nozzle/afterbody performance based upon partial-scale, wind-tunnel testing. The program includes testing of state-of-the-art single- and twin-engine fighter configurations. Due to the widespread interest in the problem being addressed, many participants have contributed to this effort to obtain an extensive wind-tunnel data base. The extent of the data base is indicated by the number of wind-tunnel test entries shown as vertical lines in Fig. 3 with triangles indicating the participants in each test.

The overall approach includes obtaining wind-tunnel data on two models of different scale and comparing these data to flight test data obtained on the same configuration. Wind-

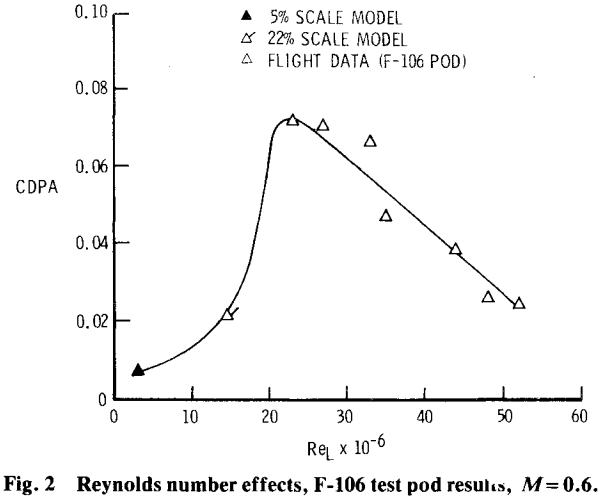

Fig. 2 Reynolds number effects, F-106 test pod results, $M = 0.6$.

tunnel data and flight test data were obtained on the YF-17 configuration at the Mach number/Reynolds number combinations indicated in Fig. 4. Thus Reynolds number effects at constant Mach number can be determined for each of the three scales. The overlap between the test conditions for the two scale models in the wind tunnel allows a determination of scale effects in the tunnel and the overlap between the 0.20 scale and flight allows a determination of wind-tunnel induced effects. A more complete discussion of the overall program objective and technical approach is presented in Ref. 3.

It was essential to provide both wind-tunnel and flight data on a common basis. Both wind-tunnel models and the flight vehicle were instrumented with surface static pressure orifices at the locations shown in Fig. 5. A more complete discussion of the orifice locations and other instrumentation is provided in Ref. 3. The use of the surface static pressure technique provides two additional benefits over the use of a force balance. First, pressure drag may be determined directly by integrating the surface static pressure distribution over the area of the afterbody and nozzle, rather than having to estimate the skin friction and subtract that value from the corrected force balance data to yield the pressure drag data. It should be emphasized that in predicting throttle-dependent nozzle/afterbody performance, it is the variation in pressure drag which is assumed to predominate. The second benefit is a substantial increase in information regarding the afterbody and nozzle flowfield. With the surface pressure distributions defined, it is possible to identify not only what the integrated effect of a variation is, but also the extent of the region where the flowfield is noticeably affected.

In evaluating the uncertainty associated with integrating the surface static pressure distribution to determine the axial load, another benefit was identified. When testing to determine the axial load applied to a partial body and using a force balance, a number of corrections must be applied to the balance measurement to account for the fact that the body is not closed: cavity pressure corrections, metric seal corrections, and base pressure corrections as shown in the first bar of Fig. 6. When the uncertainties associated with each correction are stacked together (center bar of Fig. 6) and compared to the uncertainty associated with direct integration of the measured surface static pressure, it is seen that the uncertainty associated with each case is of comparable value.[4]

Some question frequently arises regarding whether sufficient pressure orifices can be located on the model to define the pressure distribution in adequate detail to allow accurate integration. The pressure orifice density used in this program was substantially greater than that found to be sufficient on a relatively complex body of revolution tested in a different program.[1]

Scale-Model Wind-Tunnel Investigation

Tunnel Calibration

Previous tunnel calibrations were independent of the unit Reynolds number. However, upon examining the calibration data, consistent, repeatable variations of the calibration parameters with unit Reynolds number were identified. These trends were wholly within the bounds defined by the limits of the tunnel instrumentation accuracy applied to the previous Reynolds number independent tunnel calibration. Rather than neglecting the trends with Reynolds number, each test section used in this program was recalibrated and the effect of Reynolds number included in the new calibration used during this program.[5]

A comparison of the trends obtained for pressure drag of the total body, of the afterbody and nozzle, and of the forebody as a function of Reynolds number[1] with the old and new tunnel calibration is presented in Fig. 7. Data reduced

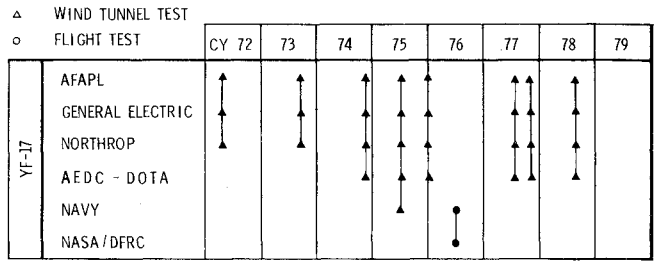

Fig. 3 Program participants and test entries.

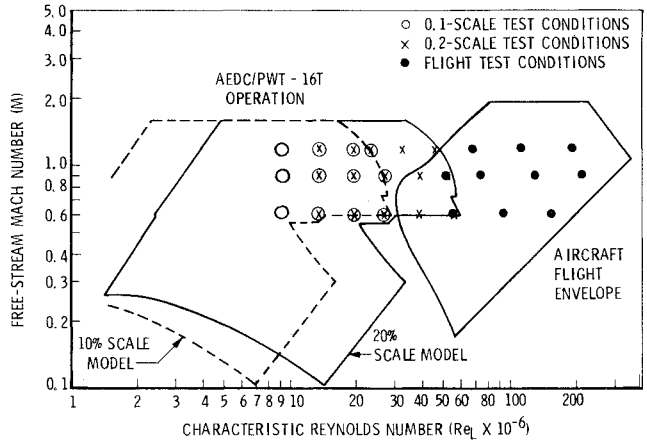

Fig. 4 Wind-tunnel and flight test conditions.

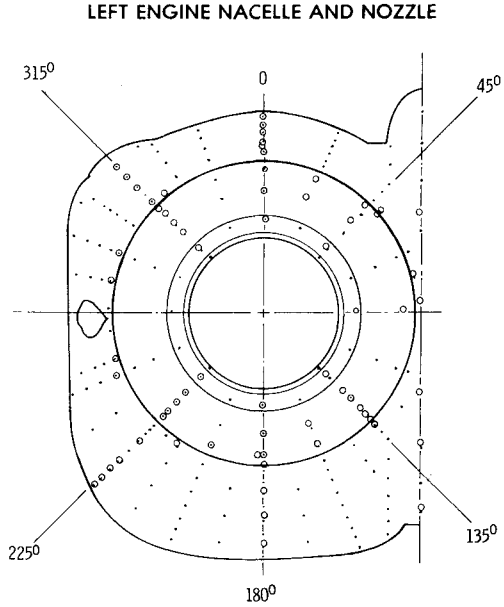

Fig. 5 Pressure orifice locations, wind tunnel (·) and flight (○).

with the previous calibration indicated a slight decrease in the total body pressure drag, while the new calibration shows this parameter to be essentially independent of Reynolds number. Of more interest to the effort described in this paper are the comparisons shown in the second and third panel of this figure. With the previous calibration, the afterbody and the forebody each erroneously indicated a significant but nearly offsetting trend with Reynolds number. With the updated calibration, the variation for each half body can be seen to be nearly independent of Reynolds number. The major deviation from the flat trend occurs at the lowest Reynolds number where the tunnel calibration is least accurate due to instrumentation accuracy limits.

Reynolds Number Effects

The surface static pressure distributions shown in Fig. 8 present the effect of varying Reynolds number for the 0.20 scale model at 0.9 Mach number.[6] These results are nearly identical to those obtained on the 0.10 scale model at the same test conditions.[7] The 180 deg row provides an excellent example of the effect of Reynolds number on a row where the flow remains attached. The greater expansion in the vicinity of the corner and the greater recompression at the trailing edge of the nozzle, which has been noted by those investigating the effect of Reynolds number variations on simple isolated bodies of revolution, is apparent.[8,9] The dashed vertical line marks the juncture between the nozzle and aircraft afterbody. The same basic trend is apparent where the flow is known to be separated (135 deg row), although the increased expansion which accompanies the increase in characteristic Reynolds number is diffused over a greater area, particularly upstream of the corner.

The effect of varying characteristic Reynolds number on the nozzle/afterbody, axial, and pressure force coefficient is shown in Fig. 9 for each of the two scales and for each of three Mach numbers. This force coefficient was obtained by integrating surface static pressure distributions like those presented in the previous figure.

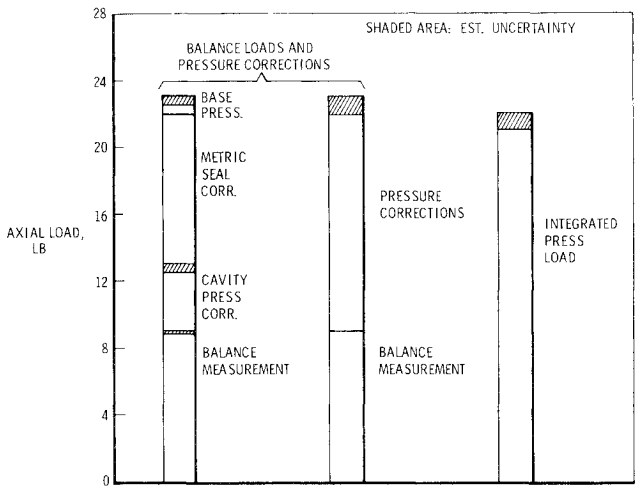

Fig. 6 Typical aft end load measurement uncertainties, effect of test technique.

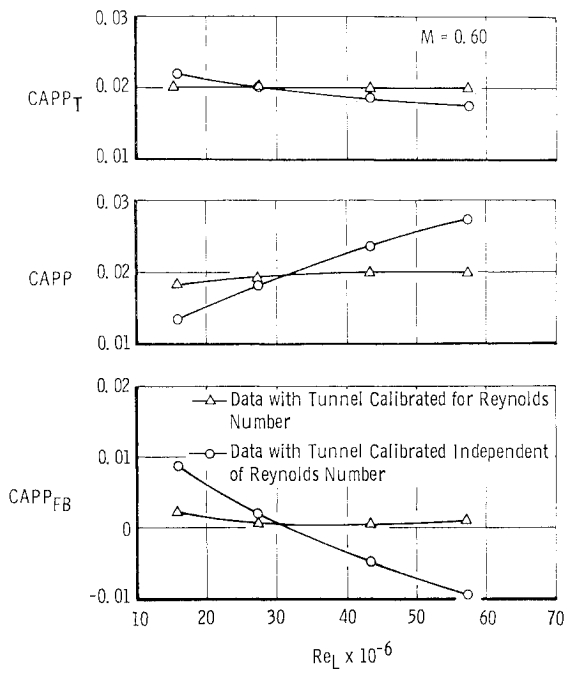

Fig. 7 Effect of tunnel calibration.

0.1 to 0.2 Scale Comparison

The top panel of Fig. 9 shows the excellent agreement between the results of the two subscale models which was obtained at subsonic Mach numbers. The second panel of this figure shows the degree of agreement which was obtained at a low transonic Mach number. At Reynolds numbers of 30×10^6 the discrepancy in integrated axial force coefficient is on the order of four drag counts (0.0004) based upon wing area and is only slightly greater at the lower limit of the Reynolds number range over which it was tested. At higher transonic Mach numbers, a substantial discrepancy between the two scales is evident, as seen in the last panel of this figure. The discrepancy seen here has not yet been resolved, although it has been hypothesized that it may be due to differences between the support system interference present in each of the two scales or interactions between the support system and the tunnel walls.

The variation of integrated axial force coefficient with characteristic Reynolds number for a nozzle setting with less closure is presented in Fig. 10. This reheat nozzle configuration is consistent with operation in the transonic region. Excellent agreement is shown at Mach numbers equal to 0.9, with the only discrepancy being at the lower limit of the Reynolds number range examined on the 0.2 scale. As noted earlier, this lower limit is most subject to accuracy problems resulting from decreased instrumentation accuracy associated with the reduced levels of absolute static pressure. In the supersonic portion of the transonic region, the discrepancy between the two scales is much less for this nozzle than for the

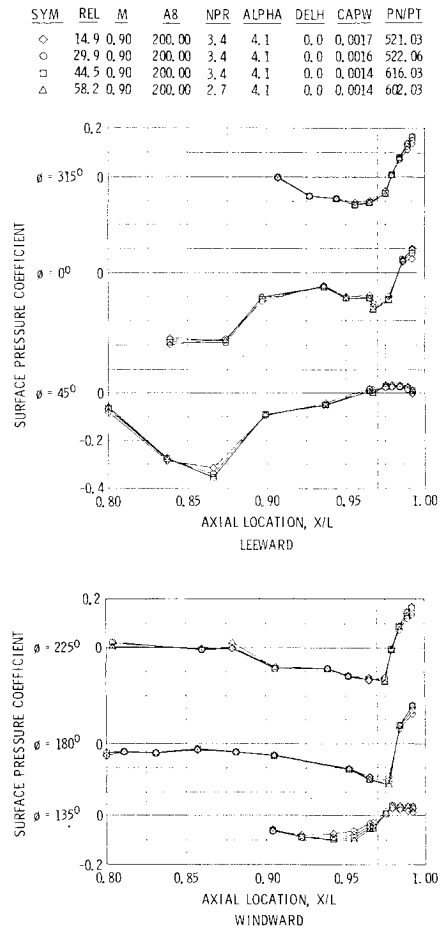

Fig. 8 Surface static pressure distribution, Reynolds number effect: wing tip supported, 0.20 scale model.

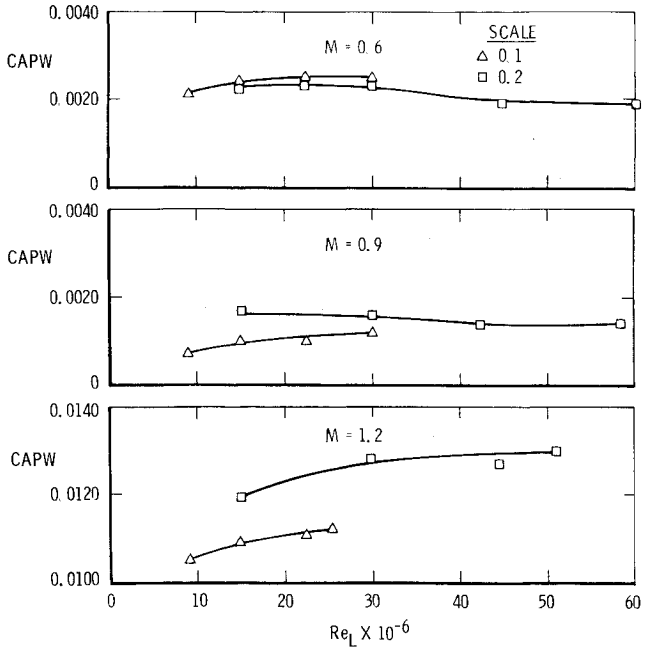

Fig. 9 Integrated axial force coefficient: wing tip supported, subscale models, cruise nozzle, design pressure ratio, $\alpha = 4$ deg, $\delta_h = 0$ deg.

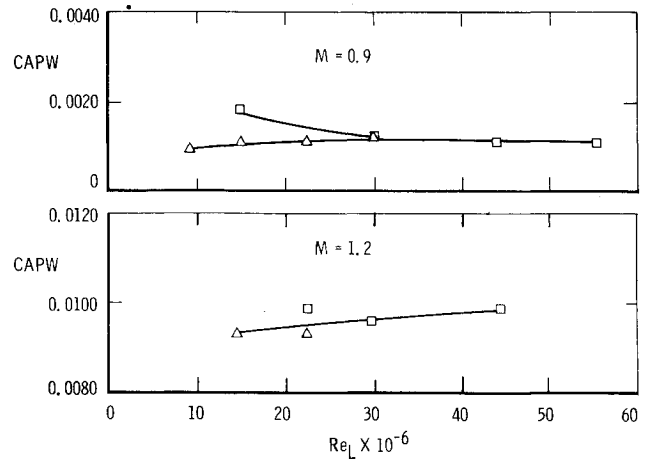

Fig. 10 Integrated axial force coefficient: wing tip supported, subscale models, reheat nozzle, design pressure ratio, $\alpha = 4$ deg, $\delta_h = 0$ deg.

nozzle with greater closure; however, data in this case are sparse.

A comparison of the surface static pressure distributions obtained on each of the two scale models at the same characteristic Reynolds and Mach numbers will allow the identification of at least some of the causes of the discrepancies between scales. For this comparison, the cruise nozzle configuration at 0.9 Mach number and 29.7×10^6 Reynolds number was selected. The surface static pressure distributions for representative rows are presented in Fig. 11. The consistency between scales is generally quite good. The anamoly at axial location $x/L = 0.80$ is probably attributable to the presence of a small step at the metric break location on the 0.10 scale model. A slight shift to lower pressure coefficients at the larger scale is evident on the inboard afterbody and nozzle. This shift is outside that attributable to instrumentation since instrumentation accuracy is indicated approximately by symbol size. Some slight discrepancies in the vicinity of the nozzle can be attributed to slight changes in

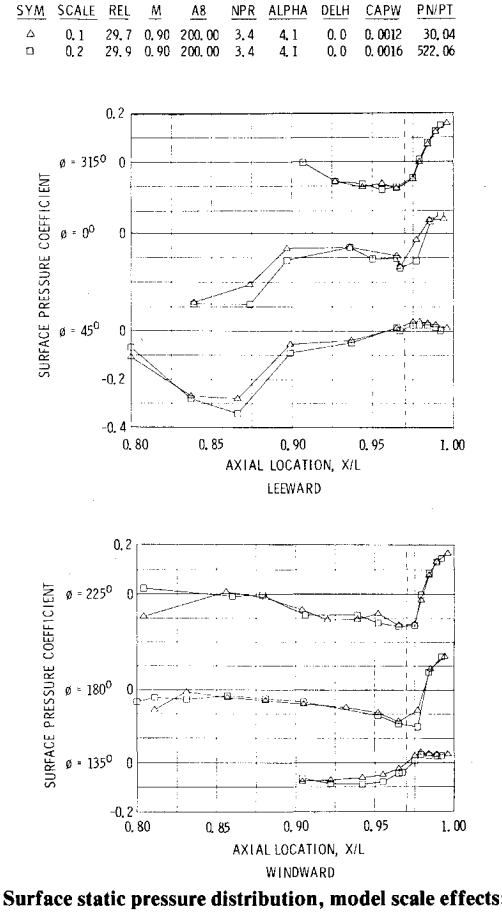

Fig. 11 Surface static pressure distribution, model scale effects: wing tip supported, subscale wind-tunnel models.

orifice location between the two scales, since this is a region of steep pressure gradient. There is a tendency for the larger scale to recompress to slightly higher levels on the unseparated region of the nozzle, although the recompression takes place further downstream.

Comparison of Wind-Tunnel and Flight Data

All data presented to this point were obtained on a wing-tip support system and include support system interference and other tunnel induced differences which would not be present in flight and for which corrections should be applied prior to comparing with data obtained in flight. The two fundamental corrections applied in the work reported here accounted for the support system interference effects[6,7] and provided interpolation between the wind-tunnel data points so that the aircraft configuration (nozzle closure, horizontal tail plane setting, etc.) and attitude (angle of attack) were very near that measured in flight.

Interpolation and Correction Procedure

Since the measurements taken in the wind tunnel were taken at specific increments rather than at the precise conditions encountered in flight, it was necessary to interpolate between a number of wind-tunnel data points in order to make a prediction of the performance at any one flight point. The method used in this effort was to interpolate between adjacent wind-tunnel points for a new value of surface static pressure coefficient at each pressure orifice. This method produced a new pressure distribution which could be compared with flight data. The advantages of this procedure are that it maintains the increased information available with the static pressure distribution, allows direct comparison with flight data, and may be integrated to provide the more traditional drag coefficient information; and an examination of the

increment in pressure coefficient due to changing any variable provides an immediate indication of the magnitude and extent of the effects of such a change. An example of the incremental effect, *DCP*, of varying nozzle closure on the pressure distribution along each of four rows is presented in Fig. 12.

Surface Pressure Distributions

A complete description of the flight test conditions, instrumentation, and vehicle has been provided previously.[3] Surface static pressure distributions are presented in Fig. 13 for four cases covering nearly one order of magnitude in characteristic Reynolds number. The wind-tunnel data has been corrected for support system interference and interpolated to match closely the flight data point which overlaps the wind-tunnel Reynolds number range. An additional flight data point is included at a much lower altitude, and subsequently much higher Reynolds number, even though it is not an exact match in variables such as nozzle pressure ratio and horizontal tail plane setting. The variation in pressure distributions due to changes in these variables of the magnitude shown here are not substantial. All rows show generally good agreement between wind-tunnel and flight data. The difference between the 0.10 and 0.20 scale model data on the 135 deg row is consistent with established Reynolds number effects; however, the flight data appear to be consistent with the 0.10 scale data on the afterbody and with the 0.20 scale data on the nozzle.

Integrated Axial Pressure Forces

Each of the surface static pressure distributions shown in Fig. 13 were integrated to determine the axial force coefficients presented in Fig. 14. For the configuration tested in this effort, no substantial effect of Reynolds number was noted at subsonic conditions.

Additional data are presented in the top two panels of Fig. 15 for subsonic and low transonic Mach numbers on the cruise nozzle configuration. Data for the reheat nozzle configuration at the higher transonic conditions are presented in the third panel of Fig. 15. The wind-tunnel data presented in these figures have been corrected to remove the support system increments; however, no interpolation has been done to match any specific flight condition. The flight data cover a range of conditions such as angle of attack, horizontal tail-plane setting, and nozzle pressure ratio. The wind-tunnel data are presented at the conditions at which the tests were conducted close to the midpoint of the flight values. The three levels of nozzle pressure ratio presented at the higher transonic Mach number show the strong influence of nozzle pressure ratio which should be considered when comparing wind-tunnel to flight data.

Conclusions

Based upon the effort conducted thus far in the program, the following conclusions have been drawn. Accurate predictions (±3 drag counts) of full-scale, flight vehicle nozzle/afterbody subsonic installation losses are within the state-of-the-art using wind-tunnel testing of subscale models. These predictions can be made using currently available facilities, test techniques, and analysis methods. However, more care should be exercised in the conduct of these tests than is routinely applied, if the improvements available are to be realized. The surface static pressure technique was judged to be superior to the method of correcting force balance data to remove estimated friction when pressure forces are the desired information and the test article is a partial body. In this case, the surface static pressure technique and the corrected force balance technique are of comparable levels of accuracy, cost, and time. The greater information available

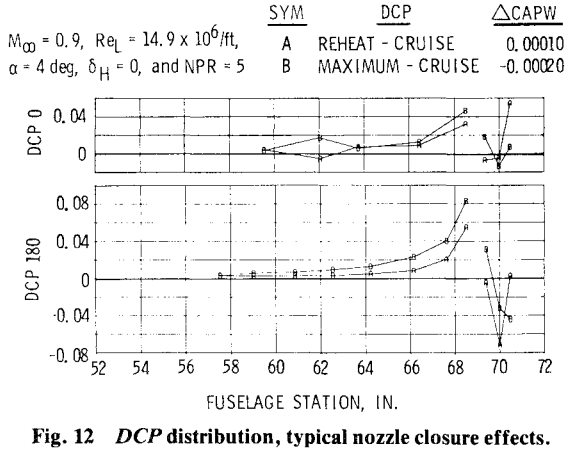

Fig. 12 *DCP* distribution, typical nozzle closure effects.

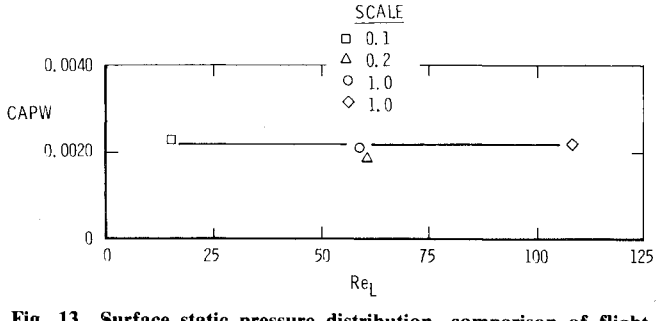

Fig. 13 Surface static pressure distribution, comparison of flight data with corrected wind-tunnel data.

SYM	SCALE	REL	M	A8	NPR	ALPHA	DELH	CAPW	PN/PT
□	0.1	14.9	0.60	200.00	3.6	6.6	-1.8	0.0023	407.02
△	0.2	60.5	0.60	200.00	3.7	6.4	-1.8	0.0019	407.04
○	1.0	58.3	0.64	205.00	3.7	6.5	-1.8	0.0021	407.03
◇	1.0	108.6	0.61	205.00	2.5	6.6	-2.0	0.0022	423.03

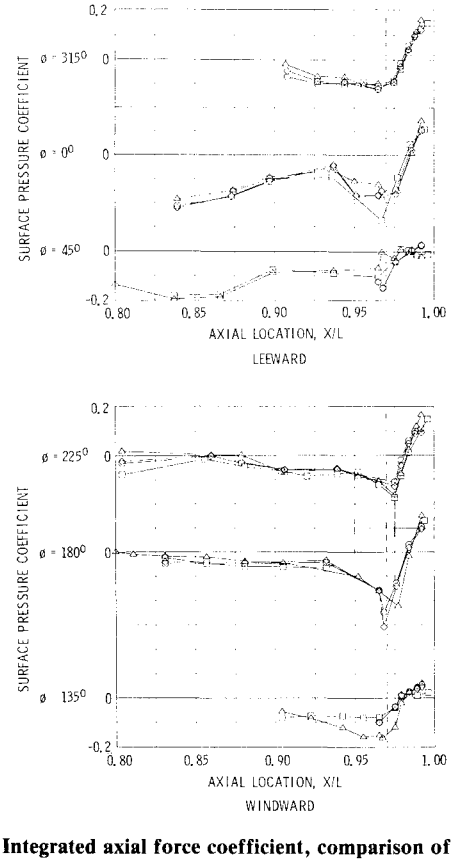

Fig. 14 Integrated axial force coefficient, comparison of flight data with corrected wind-tunnel data.

with the surface pressure distribution is the primary advantage provided, although the elimination of the uncertainty associated with estimating friction drag is also an important benefit.

For the configuration tested, the effect of increasing characteristic Reynolds number was generally a predictable increase in the depth of expansions and the height of recompressions over the entire range of Reynolds numbers examined at subsonic Mach numbers. Although this redistribution of surface static pressure was noted, the phenomenon had a tendency to be self-canceling in the integrated effect on this configuration. Only a slight change in the integrated axial drag coefficient was noted over the entire range of Reynolds numbers examined.

Recommendations

The following recommendations for wind-tunnel testing to determine nozzle/afterbody installation effects are made based upon the experience gained in this effort. Instrumentation with a substantial number of surface static pressure orifices in lieu of a force balance should be used to obtain the desired data. In addition to the greater information available as a result of using this technique, a basis for later comparison with flight test is provided. Prior to testing, an effort should be made to insure that the tunnel calibration is adequate to identify, without modification, the effects of the parameters to be examined. Even greater precision than presented in this paper is desirable for examining the effects of variables such as Reynolds number. Although testing of the configuration used in this study showed little integrated effect, this result is probably configuration dependent.[8] For this reason, it is recommended that at the initiation of testing, a variation in Reynolds number be made to substantiate whether the configuration under test is sensitive to the test Reynolds number. In tunnels which use variation in total pressure to vary Reynolds number, this may also provide the added benefit of identifying the minimum total pressure which yields acceptable accuracy on any absolute pressure transducer necessary to the test. Another item for which testing should be conducted at the beginning of any test is the support system effects. If the presence of the support system substantially alters the flowfield on the portion of the body being tested, little confidence can be placed in the absolute values of the results or even the major trends identified. It is recommended that testing to determine support system effects and Reynolds number sensitivity be performed at the initiation of the test effort, since the results of these tests should be used to modify the test plan or, in particularly bad cases, form the basis for discontinuing the test until identified problems can be resolved. Finally, the use of interpolation and corrections at each pressure orifice to remove the effects of simulation error and provide information at nontested intermediate points is recommended. This technique preserves the greater information made available through the use of the surface static pressure technique.

Although executing a test program consistent with the recommendations made here will not provide absolute certainty that the resulting predictions will be accurate, in most cases these recommendations will provide a substantial improvement over techniques currently in use.

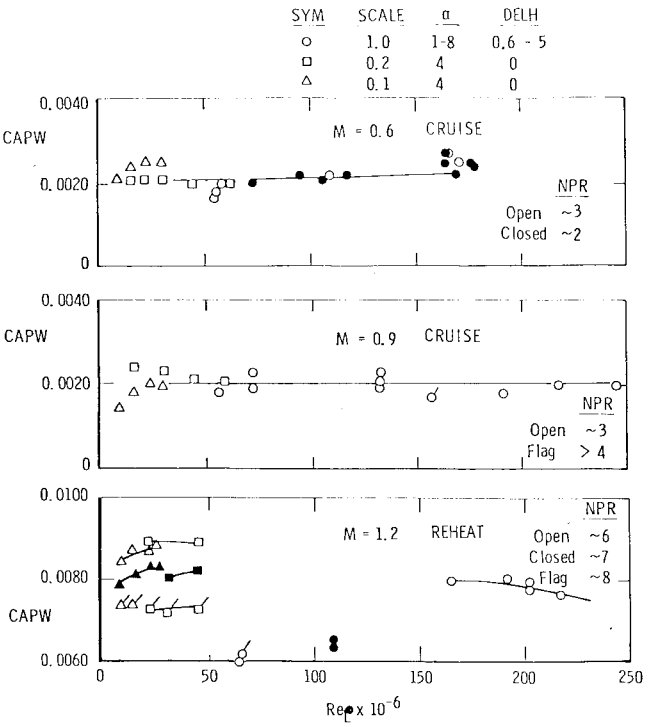

Fig. 15 Integrated axial force coefficient, comparison of flight data with corrected wind-tunnel data.

References

[1] Spratley, A.V., "An Investigation of Boattail Geometry and Reynolds Number Effects on Forebody and Afterbody Drag at Transonic Mach Numbers," AEDC TR-76-161, Feb. 1977.

[2] Wilcox, F.A. and Chamberlin, R., "Reynolds Number Effects on Boattail Drag of Exhaust Nozzles from Wind Tunnel and Flight Tests," *Airframe/Propulsion Interference,* AGARD Conference Proceedings 150, Rome, Italy, Sept. 3-6, 1974.

[3] Lucas, E.J., Fanning, A.E., and Steers, L.L., "Comparison of Nozzle and Afterbody Surface Pressures from Wind Tunnel and Flight Test of the YF-17 Aircraft," Paper 78-992 presented at 14th AIAA/SAE Joint Propulsion Conference, Las Vegas, Nev., July 1978.

[4] Schoelen, F.J., Patterson, M.W., Kostin, L.C., and Gilbertson, M., "Inlet/Nozzle Flight Performance Determination (Wind Tunnel Test Program)," AFFDL TR-78-173, April 1979.

[5] Jackson, F. M., "Calibration of the AEDC-PWT 16-Ft Transonic Tunnel Aerodynamic Test Sections at Various Reynolds Numbers," AEDC TR-78-60, Feb. 1979.

[6] Lucas, E.J., "Wind Tunnel Results from Nozzle Afterbody Test of a 0.2-Scale Fighter Aircraft in the Mach Number Regime of 0.6 to 1.5," AEDC TR-79-10, May 1979.

[7] Lucas, E.J., "Wind Tunnel Results from Nozzle Afterbody Test of an 0.1 Scale Fighter Aircraft in the Mach Number Regime of 0.6 to 1.6," AEDC TR-78-25, June 1978.

[8] Glidewell, R.J., Presz, W.M., and Stevens, H.L., "Effect of Reynolds Number and Other Parameters on the Throttle-Dependent, Nozzle/Afterbody Drag of an 0.11 Scale Simple-Engine Aircraft Model," Paper 79-1167 presented at 15th AIAA/SAE Joint Propulsion Conference, Las Vegas, Nev., June 18-21, 1979.

[9] Reubush, D. E., "The Effect of Reynolds Number on Boattail Drag," Paper 75-63 presented at 13th AIAA Aerospace Sciences Meeting, Pasadena, Calif., Jan. 20-22, 1975.